DP-1599

A GAMMA DENSITOMETER FOR MEASURING Pu DENSITY IN FUEL TUBES

WILLARD G. WINN

E. I. du Pont de Nemours & Co.
Savannah River Laboratory
Aiken, SC 29808

PREPARED FOR THE U. S. DEPARTMENT OF ENERGY UNDER CONTRACT DE-AC09-76SR00001

Printed in the United States of America

Available from

National Technical Information Service
U. S. Department of Commerce
5285 Port Royal Road
Springfield, Virginia 22161

Price: Printed Copy A04; Microfiche A01

726935

DP-1599

Distribution Category: UC - 37

A GAMMA DENSITOMETER FOR MEASURING Pu DENSITY IN FUEL TUBES

by

Willard G. Winn

Approved by:

M. L. Hyder, Research Manager
Analytical Chemistry Division

Approval Date: January 1982

E. I. du Pont de Nemours & Co.
Savannah River Laboratory
Aiken, SC 29808

PREPARED FOR THE U. S. DEPARTMENT OF ENERGY UNDER CONTRACT DE-AC09-76SR00001

ABSTRACT

A fuel-gamma-densitometer (FGD), a prototype instrument, has been developed to examine nondestructively the uniformity of plutonium in aluminum-clad fuel tubes at the Savannah River Plant (SRP). The monitoring technique is γ-ray spectroscopy with a lead-collimated Ge(Li) detector. Plutonium density is correlated with the measured intensity of the 208 keV γ-ray from ^{237}U (7d) of the ^{241}Pu (15y) decay chain. The FGD measures the plutonium density within 0.125- or 0.25-inch-diameter areas of the 0.133- to 0.183-inch-thick tube walls. Each measurement yields a density ratio that relates the plutonium density of the measured area to the plutonium density in normal regions of the tube.

The technique was used to appraise a series of fuel tubes to be irradiated in an SRP reactor. High-density plutonium areas were initially identified by x-ray methods and then examined quantitatively with the FGD. Based on calculated reactor neutron flux, acceptable density ratios could be as high as 2.00 near tube ends but had to be as low as 1.28 near tube centers. The FGD reliably tested fuel tubes against these criteria and yielded density ratios over a range of 0.0 to 2.5. FGD measurements examined (1) nonuniform plutonium densities or "hot spots," (2) uniform high-density "patches," and (3) plutonium density distribution in thin cladding regions.

The FGD performance was appraised by several tests. Measurements for tubes with known plutonium density agreed with predictions to within 2%. Attenuation measurements of the 208-keV γ-ray passage through the tube walls agreed to within 2 to 3% of calculated predictions. Collimator leakage measurements agreed with model calculations that predicted less than a 1.5% effect on plutonium density ratios. Finally, FGD measurements correlated well with x-ray transmission and fluoroscopic measurements, which are less precise, but which have been used routinely to examine plutonium density.

The data analysis for density ratios involved a small correction of about 10% for γ-shielding within the fuel tube. For "hot spot" examinations, limited information for this correction dictated a density ratio uncertainty of 3 to 5%, which is adequate for the fuel tubes examined in this study. This uncertainty existed because the modeling for tube shielding could be defined only for a range of possibilities lying between predictable maximum and minimum shielding conditions. Future "hot spot" studies may require more precise measurements, and reducing the uncertainty in plutonium density ratio by monitoring two or more γ-rays is possible.

CONTENTS

A GAMMA DENSITOMETER FOR MEASURING Pu DENSITY IN FUEL TUBES

1.0 INTRODUCTION

Plutonium fuel tubes produced at the Savannah River Plant (SRP) must meet uniformity standards before they can be placed in a reactor. These 16-foot tubes, with diameters ranging from 2.1 to 3.7 inches, are made by a coextrusion process which yields a plutonium (PuO_2-Al) cermet fuel clad with aluminum. Each tube is extruded from a billet that comprises fuel cores contained within aluminum components, as shown in Figure 1. Plutonium nonuniformities have been observed in the final ~6 inches of the extruded cores. Such "core-boundary regions" exist at the center and at one end of the fuel. The goals of the present study were to develop a prototype instrument for detailed evaluation of plutonium nonuniformities, to determine tube acceptability for reactor irradiation, and to relate nonuniformity data to specific production aspects.

The prototype instrument consists of a Ge(Li) detector that scans nominal 1/8-inch or 1/4-inch diameter circular areas of a tube for plutonium content via detection of the 208 keV gamma ray from the $^{241}U(15y) \rightarrow {}^{237}U(7d)$ decay chain.[1,2] This fuel-gamma-densitometer (FGD) supplements two existing SRP plutonium-density measuring devices that are based on x-ray transmission. One of these instruments is the fluoroscope, which is limited to semi-quantitative inspection.[3] The other, called a fuel-density-analyzer (FDA), yields quantitative densities, but only for areas equal to or larger than 1/4 inch x 1/4 inch. Furthermore, area selection with the FDA is digitized so that exact positioning for a localized maximum plutonium-density is not assured. Thus, the more detailed measurements afforded by the FGD promised to reduce the number of tube rejections resulting from the more conservative appraisals of the fluoroscope and FDA. In addition, the FGD monitors PuO_2 directly via the emitted characteristic gamma energy, while x-ray transmission measurements can only infer that the observed effects are caused by PuO_2.

The FGD has been used to study three types of PuO_2 nonuniformities observed in fuel tubes:

1. High PuO_2 density areas called "hot spots."

   The core-boundary regions are the most likely parts of the fuel tube to have any hot spots. A typical hot spot has an effective diameter $\lesssim 0.5$" and a peak PuO_2 density near the center of the spot. For sufficiently

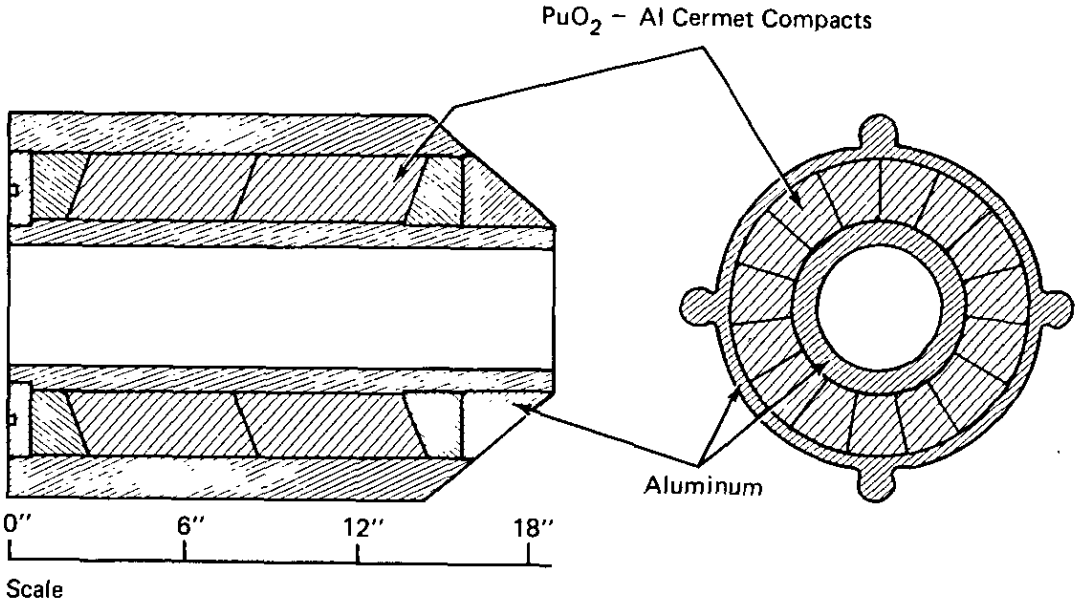

FIGURE 1. Typical Billet for Extrusion of Plutonium Fuel Tube

high PuO_2 density, these hot spots can cause accelerated corrosion of cladding and/or localized tube melting, upon irradiation in a reactor. Thus, reliable PuO_2 density measurements are required to evaluate tube acceptability.[4]

2. High uniform PuO_2 content over a large area.

   This problem can be caused by core thickening and/or by a "patch" of nonuniformly mixed PuO_2-Al. Resolution of the causal mechanism can prevent such occurrences in future tube production.

3. PuO_2 density distribution in vicinity of end core.

   The cladding thickness in the vicinity of the end core is sometimes low; however, the PuO_2 density in this region also tends to be low, in which case somewhat lower cladding thickness may be acceptable. Thus, evaluation of the PuO_2 density distribution for this region can predict the frequency of acceptable end cores for the tube manufacturing process.

Measurements on all three types of nonuniformity have been made to evaluate a series of plutonium tubes to be irradiated in an SRP reactor. For the Type 1 nonuniformity, nineteen questionable plutonium tubes were appraised for plutonium density acceptability. The results of studies on Types 2 and 3 nonuniformities were essentially guidelines for future production and acceptability criteria and did not affect acceptability of the current tube production.

Studies on the above nonuniformity types either involve FGD measurements on large, mostly uniform, but high density regions or on smaller regions of highly nonuniform density. Both types of regions were identified qualitatively from x-radiographs. Gamma-densitometer systems have been used previously to measure plutonium densities and/or content with precision <2% over large, slowly varying densities.[5-16] Typically these studies used collimator diameters much greater than 1/8 inch, plutonium calibration sources or fuel rods, and attenuation corrections based on uniformly distributed plutonium. With the FGD, uniform densities are measurable with comparable precision of ~2%, although the smaller 1/8- or 1/4-inch-diameter collimators do not average out small density fluctuations. For the hot spot measurements, a somewhat worse precision of 3 to 5% is dictated by attenuation uncertainties associated with the uncertainty of the PuO_2 distribution within the hot spot. This uncertainty results because the x-radiographs of hot spot areas are too varied to infer much about PuO_2 depth distribution within the hot spot. This depth information would be used in attenuation modeling to obtain a correction factor. In spite of this, the overall precision afforded by the FGD is more than adequate for the appraisals required to determine acceptability of the fuel tubes for irradiation.

2.0 TECHNIQUE

2.1 Overview

Figure 2 provides a schematic description of the FGD technique. Measurements were performed for three types of fuel tubes, having dimensions given in Table I. (The tube types are labeled "outer," "middle," and "inner" to denote their concentric locations within a fuel assembly). Fuel tube areas of 1/8-inch or 1/4-inch diameter are scanned by a 55-cm^3 Ge(Li) detector collimated by lead. A lead plug placed within the fuel tube shields the detector against gamma rays from the far side of the tube. In a typical measurement, the 208 keV gamma ray resulting from the approximately 2% isotopic fraction of ^{241}Pu is counted first for a normal area of the tube and then for the high density area in question. The ratio of these two count rates, when corrected for gamma-shielding, yields a measure of the relative fuel density of the desired area.

2.2 Theoretical Basis

The success of this method is primarily due to properties of the 208 keV gamma ray from ^{241}Pu, which monitors the PuO_2 content. First, the 208 keV gammas produce a prominent clean peak in the Ge(Li) spectrum, as indicated in Figure 3. Secondly, these gammas are well shielded by the lead of the collimator and tube plug. Finally, they are not strongly attenuated by the PuO_2-Al tube. This results because, even though plutonium is a stronger gamma absorber than lead, the plutonium content of the fuel tube is relatively small compared to the host aluminum, which is a weak gamma absorber.

For best results, the 208 keV gamma count rates must be corrected for attenuation by the tube. Different attenuation correction models must be applied to (1) a count rate R_0 measured for a uniform tube region and (2) a count rate R measured for a nonuniform (hot spot) region. R_0 results from a uniform distribution of PuO_2 within the fuel annulus, as shown in Figure 4. R can result from a variety of PuO_2 distributions which lie between extreme cases shown in Figure 5. These extreme cases have all the PuO_2 concentrated either at the inner or outer boundary of the fuel annulus. For the respective extremes of Figure 4a and 4b, the same count rate, R, is produced by minimum and maximum amounts of PuO_2, corresponding to minimum and maximum attenuation of the detected gamma.

Referring to Figure 4, R_0 resulting from the PuO_2 source C_0, as viewed by the collimated detector, is given by:

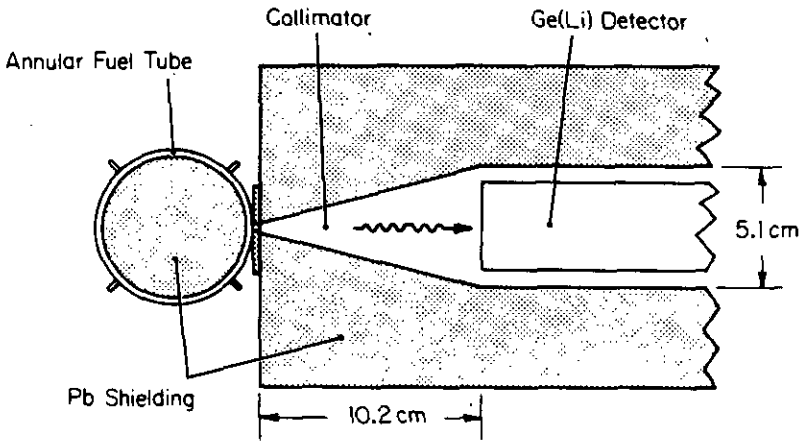

FIGURE 2. Basic Measuring Techniques with Fuel-Gamma-Densitometer

TABLE I

Fuel Tube Parameters*

Tube	O.D. (in)††	t_c** (in)††	t_o (in)††	t_c'** (in)††	χ	f_p†	ρ_0 (gm/cm^3)
Inner	2.084	0.030	0.113	0.040	0.9466	0.0483	0.524
Middle	2.936	0.030	0.113	0.030	0.8466	0.0727	0.700
Outer	3.700	0.030	0.073	0.030	0.8504	0.0606	0.590

$\mu a = 0.324\ cm^{-1}$ $\mu_p = 13.21\ cm^{-1}$

* Refer to Figure 4 and Equation 1 and 2.

** Design values are given, but values 0.008 inches lower are acceptable. The maximum associated effect on R and R_0 measurements is <0.6% and thus is neglected.

† Using f_p, the value $f_a = 1 - f_p$ is calculated.

†† Values given in inches, from the drawings. These are converted to cm before using with calculation formulae.

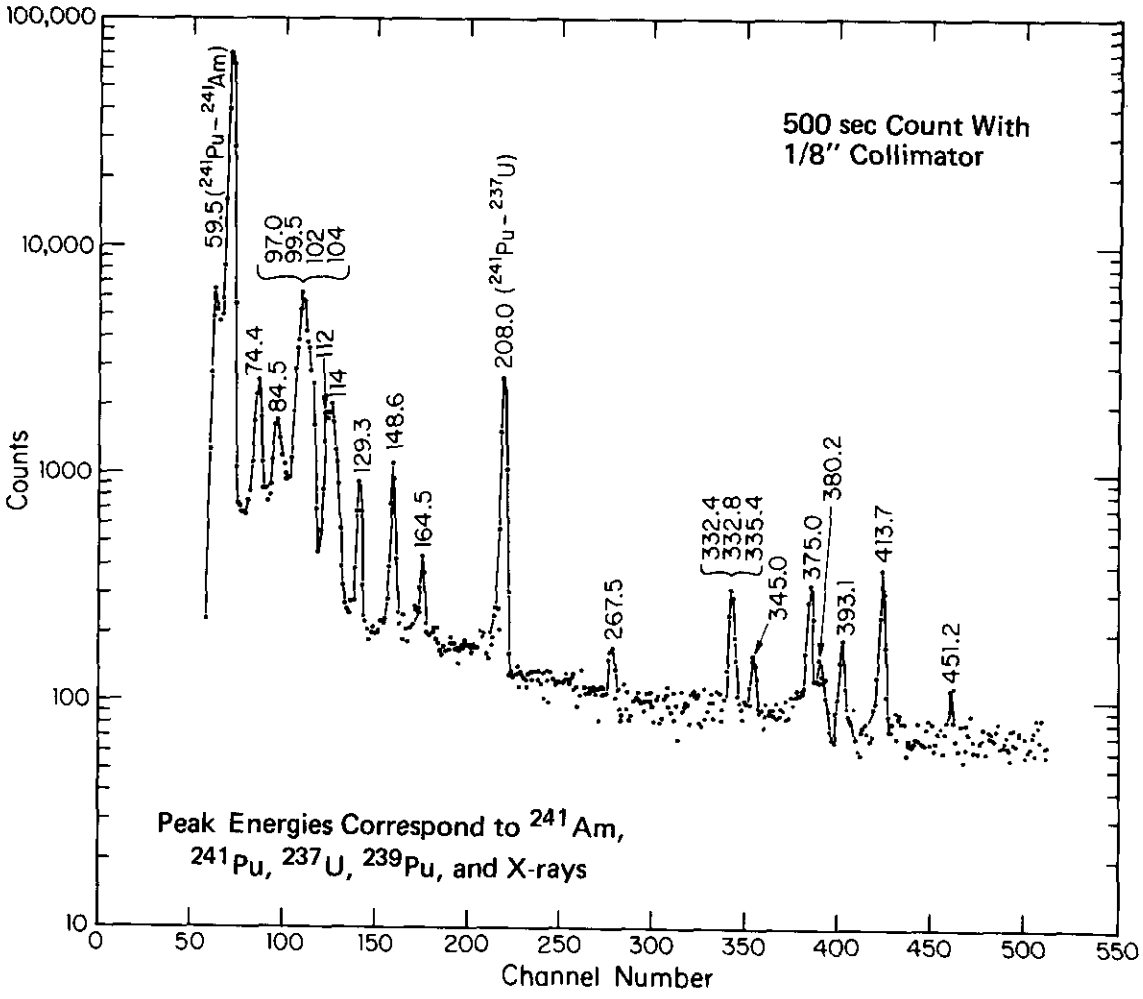

FIGURE 3. Typical Ge(Li) Spectrum of PuO_2-Al fuel tube

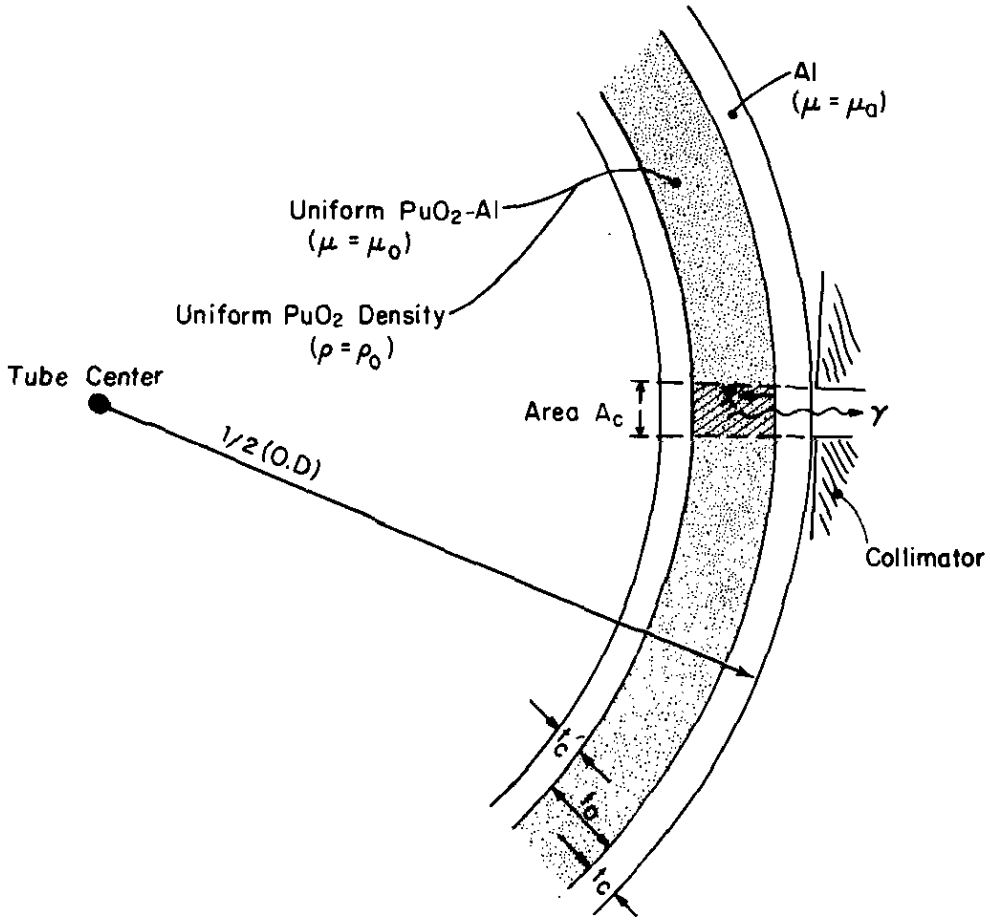

FIGURE 4. Fuel Tube and Collimator Geometry for Uniform Tube Areas. Gamma Rays are Detectable From Shaded Region of Volume $A_c t_0$, Containing PuO_2 Source $C_0 = \rho_0 A_c t_0$

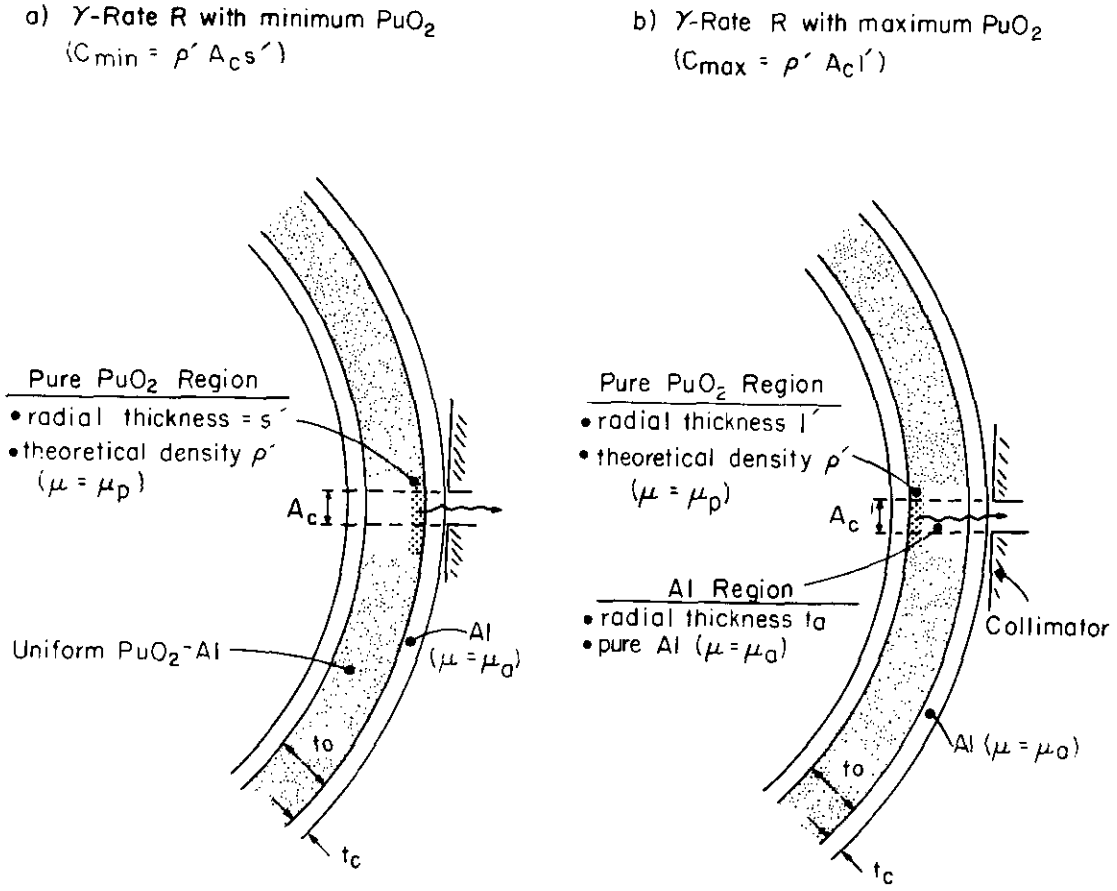

FIGURE 5. Extreme Possibilities for Geometry of Nonuniform Abnormality

$$R_0 = e^{-\mu_a t_c} \int_0^{t_0} e^{-\mu_0 x} \varepsilon \rho_0 A_c dx$$

$$= C_0 \varepsilon e^{-\mu_a t_c} \frac{1 - e^{-\mu_0 t_0}}{\mu_0 t_0} \qquad (1)$$

where:

x = distance into fuel annulus (cm)

t_0 = thickness of fuel annulus (cm)

A_c = collimator entrance area (cm^2)

ρ_0 = PuO_2 density (gm/cm^3)

$C_0 = \rho_0 A_c t_0$ = PuO_2 source viewed by detector (gm)

ε = unattenuated 208 keV detection rate/unit of PuO_2 (counts/sec/gm)

t_c = thickness of outer aluminum cladding (cm)

μ_a = aluminum attenuation coefficient for 208 keV gamma (cm^{-1})

μ_0 = fuel annulus attenuation coefficient for 208 keV gamma (cm^{-1})

In addition, μ_0 is given by

$$\mu_0 = \chi(f_a \mu_a + f_p \mu_p) \qquad (2)$$

where:

χ = fraction of theoretical density of PuO_2-Al (unitless)

f_a = volume fraction of aluminum (unitless)

f_p = volume fraction of PuO_2 (unitless)

μ_p = PuO_2 attenuation coefficient for 208 keV gamma (cm^{-1}).

Values of μ_a and μ_p correspond to 100% theoretical densities and were obtained from tabulations.[17] Other parameters were obtained from fuel design specifications and/or fabrication measurements, some of which are given in Table I.

Referring to Figure 5a, R resulting from a minimum PuO_2 source C_{min} is given by

$$R = e^{-\mu_a t_c} \int_0^{s'} e^{-\mu_p x} \varepsilon \rho' A_c dx$$

$$= C_{min} \varepsilon \, e^{-\mu_a t_c} \, \frac{1 - e^{-\mu_p s'}}{\mu_p s'} \qquad (3a)$$

where the new parameters are:

x = distance into pure PuO_2 annulus (cm)

s' = thickness of pure PuO_2 annulus (cm)

ρ' = theoretical density of pure PuO_2 (gm/cm^3)

$C_{min} = \rho' s' A_c$ (gm)

Similarly, referring to Figure 5b, R resulting from a maximum PuO_2 source C_{max} is given by:

$$R = e^{-\mu_a (t_c + t_a)} \int_0^{\ell'} e^{-\mu_p x} \varepsilon \rho' A_c dx$$

$$= C_{max} \varepsilon \, e^{-\mu_a (t_c + t_a)} \, \frac{1 - e^{-\mu_p \ell'}}{\mu_p \ell'} \qquad (3b)$$

where new parameters are:

ℓ' = thickness of pure PuO_2 annulus (cm)

t_a = attenuation thickness of Al in fuel annulus (cm)

$C_{max} = \rho' \ell' A_c$

Again, we emphasize that the same R may be produced by a range of PuO_2 sources lying between C_{min} and C_{max}, which correspond to possible minimum and maximum attenuation from the fuel tube.

Comparison of one fuel area to another is made by measuring the count rate of each area, appraising whether R_0 or R modeling is appropriate for shielding corrections, and then ratioing the count rates. When any of the expressions (1), (3a), or (3b) are ratioed to each other, factors of ε and A_c will cancel, making their explicit determination unnecessary.

The count rates are usually ratioed to R_0^N, the count rate for a normal design region of the tube. For hot spot examination ratio R/R_0^N, is useful because it yields the density ratio $D = C/C_0^N$, which measures the PuO_2 concentration of an abnormal area relative to a normal tube area. Using Equations 1 and 3, we have:

$$D_{min} = \frac{C_{min}}{C_0^N} = \frac{\rho' s'}{\rho_0^N t_0} = \frac{R}{R_0^N} \frac{\left(1-e^{-\mu_0 t_0}\right) \mu_\rho s'}{\left(1-e^{-\mu_\rho s'}\right) \mu_0 t_0} \qquad (4a)$$

$$D_{max} = \frac{C_{max}}{C_0^N} = \frac{\rho' \ell'}{\rho_0^N t_0} = \frac{R}{R_0^N} \frac{\left(1-e^{-\mu_0 t_0}\right) \mu_\rho \ell'}{\left(1-e^{-\mu_\rho \ell'}\right) \mu_0 t_0} e^{\mu_a t_a} \qquad (4b)$$

For any given value of R/R_0^N, ℓ' and s' can be determined, as all other parameters in Equations (4) are known*. Then D_{min} and D_{max} may be calculated as a function of R/R_0^N. A simple BASIC computer program performed these calculations, yielding results as $D \pm \Delta D$, where $D = \frac{D_{max} + D_{min}}{2}$ and $\Delta D = \frac{D_{max} - D_{min}}{2}$. For the fuel tubes examined, Figure 6 indicates that D essentially agrees with the measured ratio when $R/R_0^N < 1$, but grows steadily larger (~10% larger for $R/R_0^N = 2$) as R/R_0^N increases. The value of ΔD is 3 to 5% of D for these tubes; thus, the model uncertainties associated with the shielding corrections do not seriously limit the method. Other uncertainties in D, such as those in nuclear statistics, geometry variations, and gamma spectral analysis, are small relative to ΔD in all reported measurements.

When comparing regions of uniform density, two R_0 values are ratioed. Here each R_0 predicts a unique C_0 (as opposed to values ranging between C_{min} and C_{max} for R measurements), and therefore the corresponding density ratio $D_0 \pm \Delta D_0$ is much better defined than the typical $D \pm \Delta D$. Because PuO_2 distribution uncertainties are absent for R_0 analyses, $\Delta D_0 \lesssim 2\%$ results, as dictated by the precision of the two R_0 measurements.

---

* Note: $t_a = t_0 - \ell'$

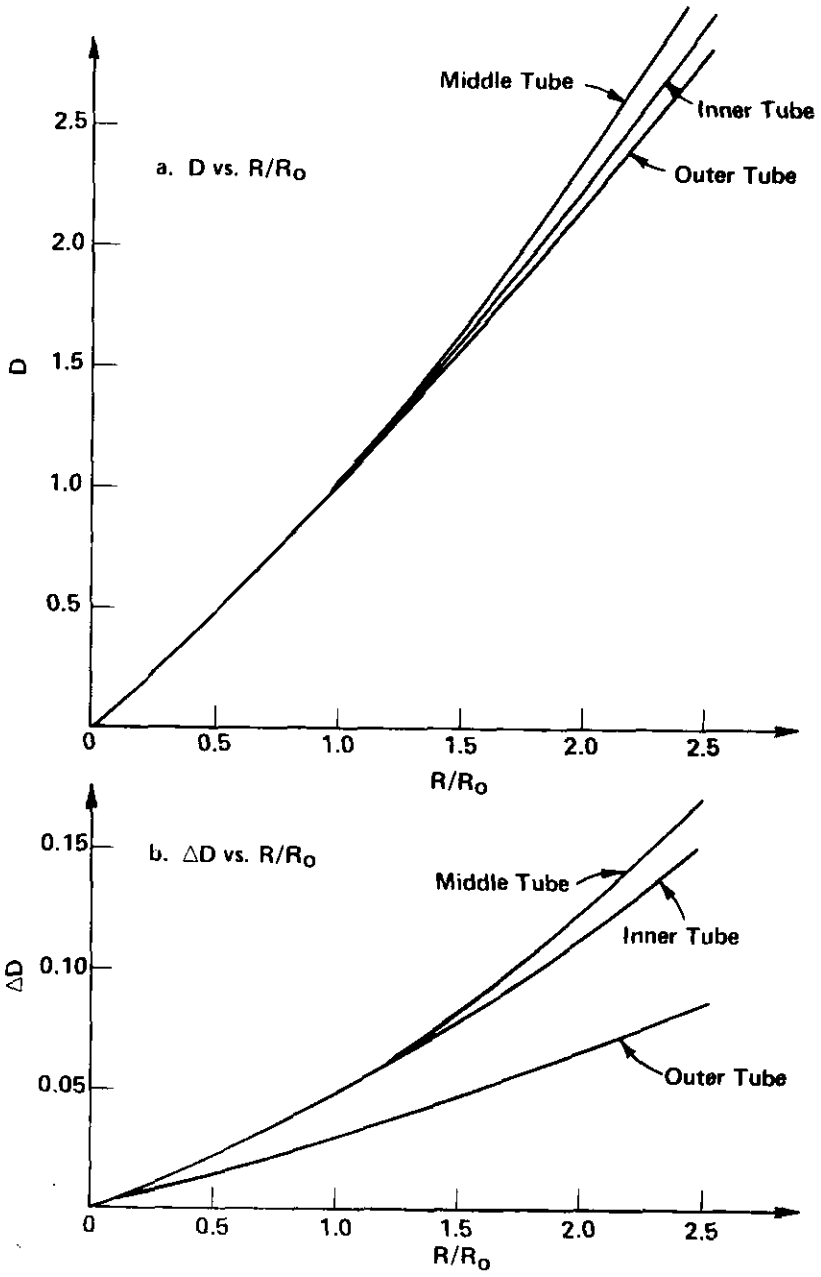

FIGURE 6. D and ΔD for R/R_0 Measurements of "Hot Spots"

2.3 Instrumentation

Figure 7 is a photograph of the equipment outlined in Figure 2. The main features are the lead shielding, tube positioning features, and the γ-monitoring system.

Ideally, the lead shielding must eliminate from detection all γ-rays that are not emitted from the area being monitored. For the tubes examined in this work, this means that over 99.9% of the fuel tube must be shielded. This is accomplished by providing four inches of lead shielding around the Ge(Li) detector, except in the vicinity of the collimator entrance. The lead-attenuation coefficient for the 208 keV gamma rays is 10 cm^{-1}, meaning that one inch of lead reduces the γ-intensity by a factor of approximately 10^{11}. Also, gammas from the far side of the tube, which could be detected via the collimator, are shielded by lead tube inserts at least 1.5 inches in diameter.

Normally, the tube area tested is placed directly against the collimator entrance so that gammas from surrounding areas are shielded. Because some of the tubes required measurements for areas near tube ribs, a special lead-shimming technique, shown in Figure 8, was developed for suitable shielding in these cases. Without the shims, the rib would displace the desired tube area away from the collimator entrance, causing a much larger area to be seen by the Ge(Li) detector. One of the shims is an extension of the collimator entrance window. Either 1/8-inch or 1/4-inch-diameter windows were defined by these shims. (The conical collimator itself had an entrance of 1/4-inch diameter.)

Tube areas to be examined by the FGD were initially identified by the fluoroscope and/or x-radiography. The areas for FGD inspection were identified on each tube with a marking pen. The marked area was then covered by a piece of 1/10-inch-grid transparent graph paper to aid placement in front of the collimator window (see Figure 9). A similar piece of graph paper attached to the collimator acted as a positioning guide. In those cases where the area to be investigated was a hot spot, the graph paper technique also provided a convenient way to map the peak density of the spot, to confirm or correct the location given by the marking pen.

The γ-monitoring system is composed of a 55-cm^3 Princeton Gamma Tech Ge(Li) detector with preamp, an ORTEC Model 452 Spectroscopy Amplifier, and a Canberra 8100 multichannel analyzer. The detection efficiency of this system was generally capable of counting the 208 keV gamma with about 1% statistics in <1000 sec with the 1/8-inch-diameter collimator. Peak areas for the gamma ray were determined using the integral windows features of the multichannel analyzer.

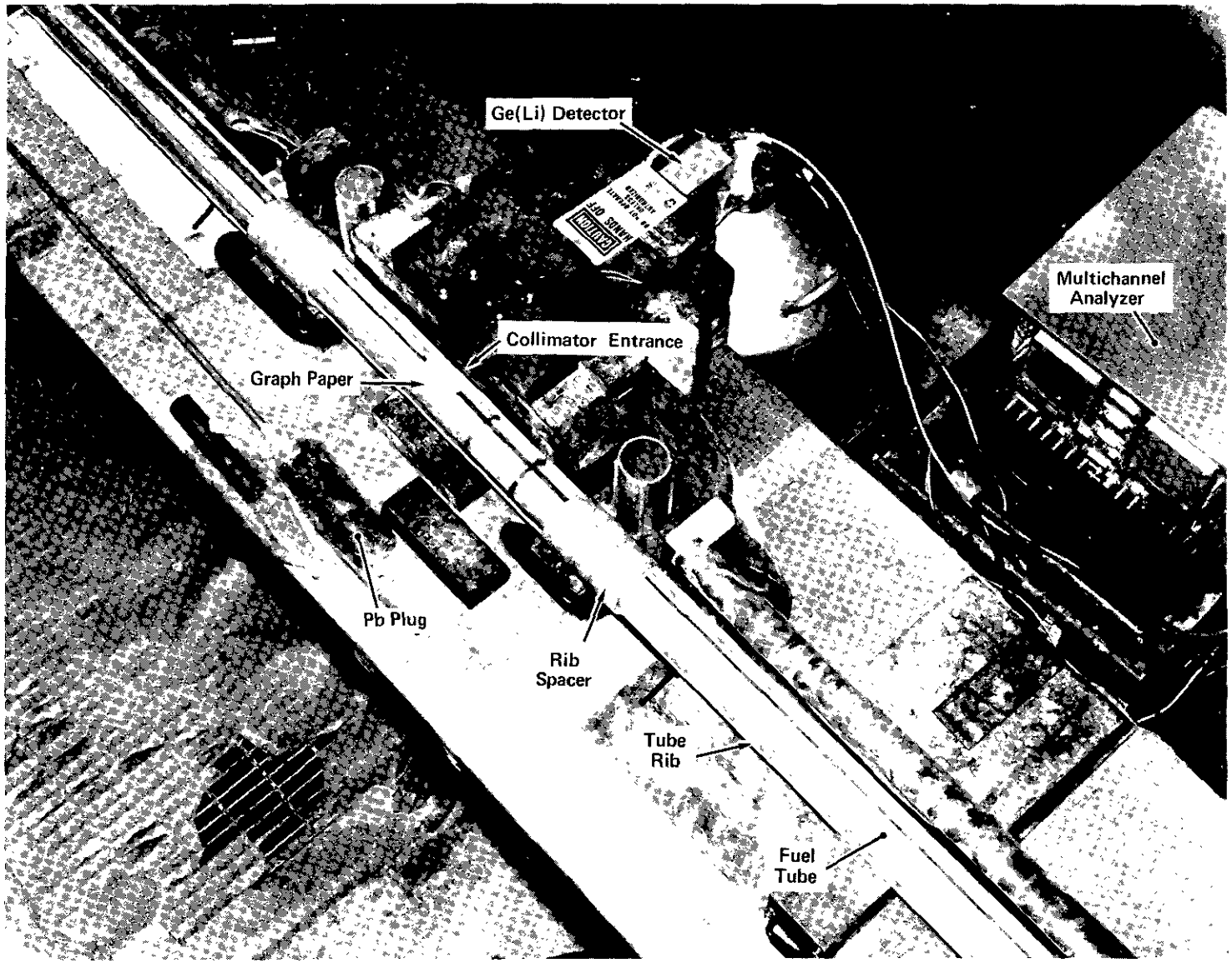

FIGURE 7. FGD Instrumentation

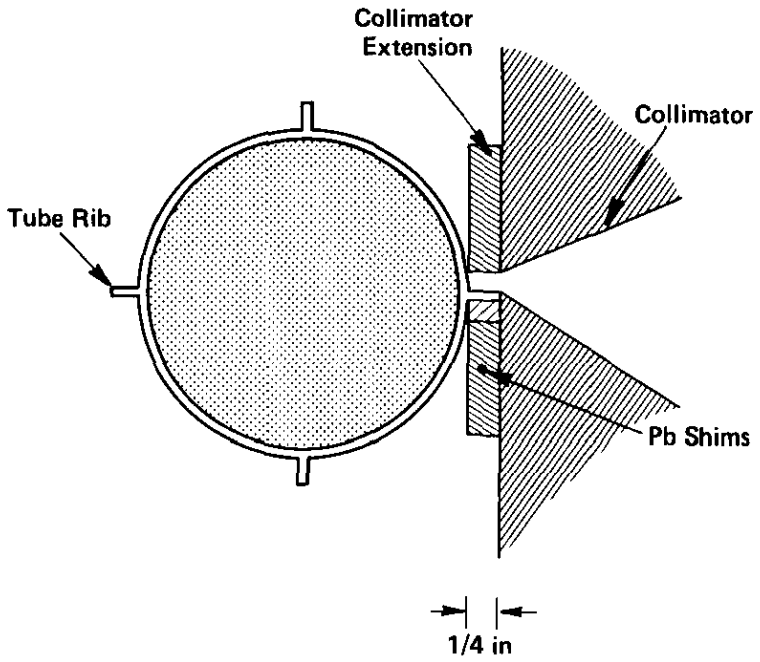

FIGURE 8. Pb-Shims for Shielding Rib Regions of Fuel Tubes

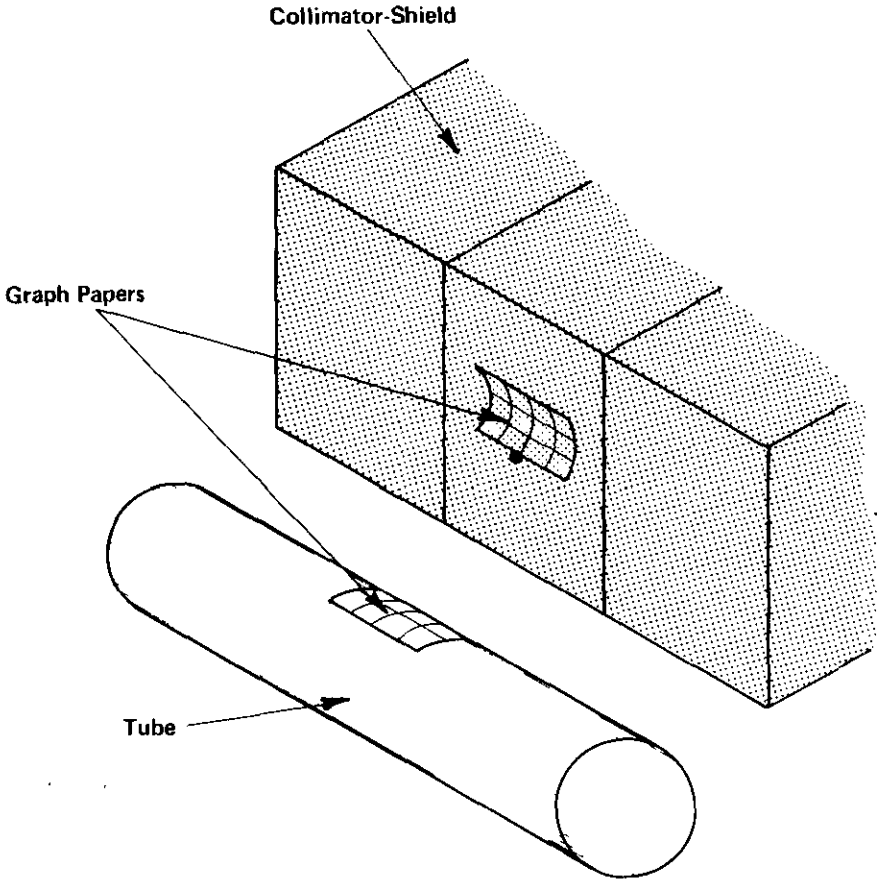

FIGURE 9. Techniques for Positioning Tube Areas

2.4 Measurements

A typical density measurement for a hot spot requires a gamma count rate R at the marked tube area and a count rate R_0^N at a normal design density area of the tube. Actually, several normal tube areas are counted during the course of measuring the densities of the marked areas of the tube. The normal area measured initially is recounted as a final check, to confirm that the instrument was stable during the measurements.

Measurement of R typically involves two steps. First, the count rates at several locations associated with the grid over the marked area are determined. Results of such a measurement are given in Figure 10, where 50-sec counts with a 1/8-inch collimator yield counting statistics (<4%) for the peak density location to be identified. Gamma windows at 60 keV and 208 keV are used to verify the peak location (see Section 5.2 for discussion of 60 keV gamma). After the peak position is determined, a longer count (1000 sec) is taken at this location to determine the value of R.

For measurements of uniform densities, count rate mapping is unnecessary.

2.5 Analysis

Ratios for R and R_0 measurements are determined and then corrected for attenuation effects using the formulae of Section 2.2. Inputs for these calculations are the R, R_0, and R_0^N measurements and the material and geometry features of the tube summarized in Table I.

The $D \pm \Delta D$ analyses of hot spots are designed to yield Pu densities that are conservatively high. In particular, R_0^N is chosen as the minimum count rate of several normal tube areas examined. This reduces the probability of getting a slightly larger ($\lesssim$0.6%) R_0^N due to acceptable cladding thinning (Table I, Footnote ††). At the same time, R is selected as the maximum R determination. Thus, R/R_0^N and $D \pm \Delta D$ will be the largest values scoped by the data. In typical measurements, the counting statistics and cladding fluctuations indicate that the above conservatism yields D values that are high by less than 2%.

The $D_0 \pm \Delta D_0$ analysis of uniform high density areas is essentially identical to that for $D \pm \Delta D$.

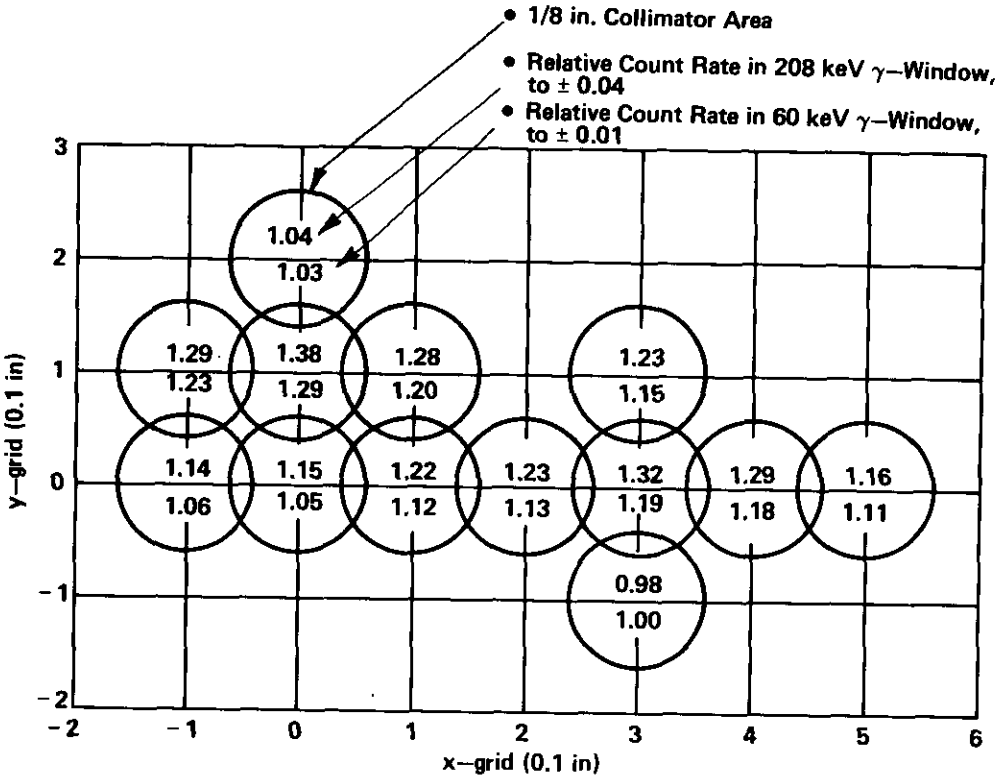

FIGURE 10. Example Mapping of Count Rate for Inner Tube. Peak Density of "Hot Spot" is at (0,1). The Mapping with 208 keV Window Yields a More Pronounced Maximum Than That of the 60 keV Window, Because of Self-Shielding Effects.

3.0 PERFORMANCE TESTING

The FGD operational performance was appraised by (1) comparing areas of known PuO_2 density, (2) measuring tube attenuation features associated with the calculation of D and D_0, (3) examining collimator leakage, and (4) comparing FGD measurements with FDA and fluoroscope results. Each of these approaches is discussed in detail below.

3.1 Areas Of Known PuO_2 Density

Measured and calculated R_0^N for inner, middle and outer fuel tubes can be compared, because the corresponding PuO_2 densities are known. Using the information of Table I, the R_0 for each tube is calculated in terms of ε using Equation 1. While ε does not have to be known exactly, the relative ε value for each tube is determined from the ratios of known ^{241}Pu enrichment. By using measured and calculated R_0/ε, the enrichment discrepancies are normalized so that all tubes can be compared readily.

Table II compares measured and calculated R_0/ε for the three tube sizes. Here, the measurements are averages of R_0/ε for each size tube. The agreement between measurement and calculation is very good and within the ~2% precision of the measurements.

3.2 Tube Attenuation

Total attenuation of the tube walls was measured as a check on the attenuation coefficients used in calculating D and D_0. The wall attenuation is measured in a normal region of the tube by using count rates R_0^N and R_0^{N0}. R_0^{N0} is the count rate with the lead plug removed from the tube. Thus, $R_0^{N0} - R_0^N$ is the count rate contributed from the far side of the tube. Referring to Figure 11 and Equation 1, we have

$$R_0^{N0} - R_0^N = \left(e^{-2\mu_a t_c'} - \mu_{0\,t_0} - \mu_a t_c\right) \int_0^{t_0} \left(e^{-\mu_0 x}\right) \varepsilon \left(d_1/d_2\right)^2 \rho_0 \, A_c \left(d_2/d_1\right)^2 dx$$

$$= \left(e^{-2\mu_a t_c'} - \mu_0 t_0\right) R_0^N \qquad (5a)$$

TABLE II

Measured and Calculated R_0/ε

	R_0^N/ε (relative units)		
Tube	Calculated*	Measured**	Measured/Calculated†
Inner	1.000	1.006 ±0.013	1.006 ±0.013
Middle	1.307	1.300 ±0.032	0.995 ±0.024
Outer	0.758	0.750 ±0.015	0.989 ±0.020
Average	-	-	1.000

* R_0/ε values relative to inner tube (R_0/ε = 1.000). Calculation with Equation 1, using data from Table I.

** From 1/8" - collimator measurements, normalized to inner tube (R_0/ε = 1.006 ±0.013), per discussion in the last footnote.

† Normalized so that average (weighted with respect to error) equals 1.000.

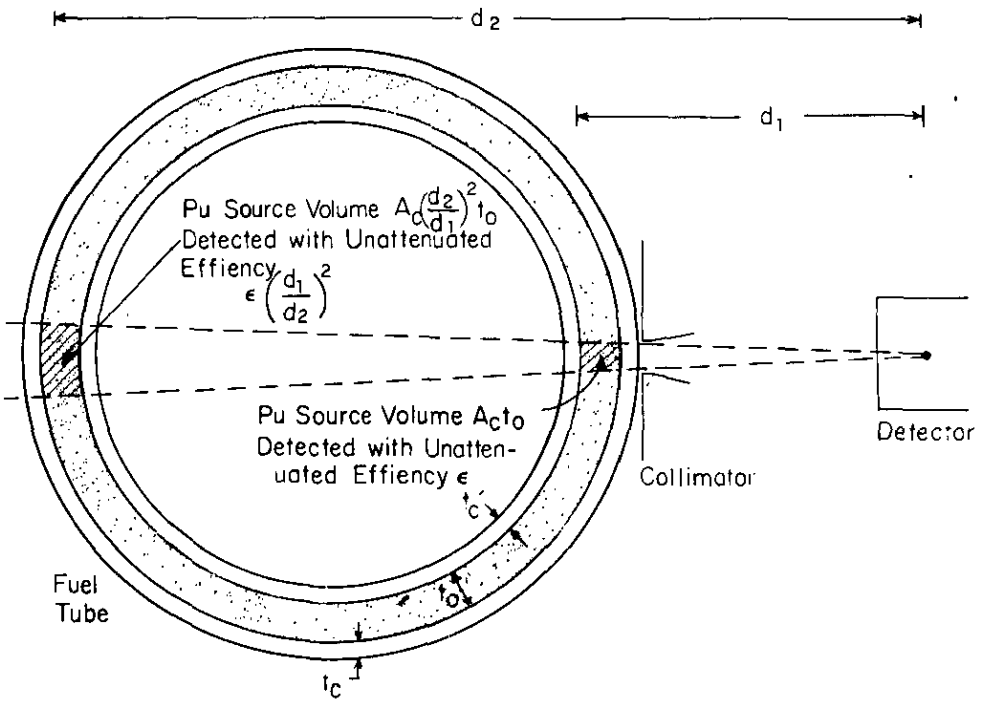

FIGURE 11. Gamma Sources Detected With No Lead Shield Within Fuel Tube

where:

t_c' = inner clad thickness (cm)

d_1 = effective distance from detector to near side of fuel tube (cm)

d_2 = effective distance from detector to far side of fuel tube (cm)

Rearranging Equation 5a yields,

$$e^{-2\mu_a t'_c} - \mu_0 t_0 = \frac{R_0^{N0} - R_0^N}{R_0^N} \qquad (5b)$$

Thus, measured values of R_0^N and R_0^{N0} are used to appraise the calculated attenuation factor of $e^{-2\mu_a t'_c - \mu_0 t_0}$.

Attenuation measurements for the fuel tubes studied are compared with calculations in Table III. The agreement is within the measurement error of 2 to 3% and infers that appropriate attenuation modeling is used.

3.3 Collimator Leakage

Measurements were made to check the collimator leakage predicted by model calculations. The R/R_0^N measurements for hot spots are of primary concern, because leakage can reduce the spatial resolution of the collimator and thus yield a low R/R_0^N. The effect of collimator leakage on R/R_0^N measurements is evaluated by examining

$$R/R_0^N = \frac{\int_0^\infty \varepsilon(r)\ \sigma(r) 2\pi r dr}{\int_0^\infty \varepsilon(r)\ \sigma_0^N\ 2\pi r dr} \qquad (6)$$

where:

r = radial distance from collimator axis

$\sigma(r) = \int_0^{t_0} e^{-\mu x} \rho(x) dx$ = effective PuO_2 source/unit area

$\sigma_0^N = \int_0^{t_0} e^{-\mu_0 x} \rho_0 dx$ = $\sigma(r)$ for normal tube regions

$\varepsilon(r)$ = ε as a function of r.

TABLE III

Tube Attenuation Appraisal

Tube	Attenuation	
	Calculated* = $e^{-2\mu_a t'_c - \mu_0 t_0}$	Measured** = $\frac{R^{N0}_0 - R^N_0}{R^N_0}$
Inner	0.726	0.727 ±0.015
Middle	0.697	0.720 ±0.020
Outer	0.810	0.797 ±0.017

* Using data from Table I.
** Averages from measurements for several tubes.

In the above expression $\varepsilon(r)$, the unattenuated detection efficiency per unit of PuO_2, has the primary influence on the measured R/R_0^N. For a collimator of radius a, the ideal case with no leakage has

$$\varepsilon(r) = \text{constant} > 0 \text{ for } r \leq a \qquad \text{(ideal)}$$

$$0 \text{ for } r > a$$

By contrast, the actual case has:

$$\varepsilon(r) > 0, \text{ for } 0 < r < \infty \qquad \text{(actual)}$$

In the actual case, collimator leakage exists because a finite detection efficiency exists for fuel tube points with r>a, which are outside the collimator window. The ideal and actual $\varepsilon(r)$ are modeled in Figure 12a, using the geometrical dimensions for the source, collimator, and detector.

The source distribution $\sigma(r)$ of Equation 6 was modeled as:

$$\sigma(r) = \sigma_0^N \left(1 + \alpha e^{-r^2/2h^2}\right) \qquad (7)$$

where:

α = maximum relative deviation of tested area from normal tube areas

h = Gaussian parameter = FWHM/2.355

This model of $\sigma(r)$ assumes that any tested region is composed of a normal tube density σ_0^N plus an abnormal density which is distributed as a Gaussian "bump". Furthermore, it is assumed that the peak of this bump is centered in the collimator window during R measurements. These assumptions are supported by the density mappings discussed in Section 2.4.

In Figure 12b, R/R_0^N is plotted as a function of the full width at half maximum (FWHM) of a Gaussian distribution for the ideal and actual $\varepsilon(r)$. Here, R/R_0^N is calculated using Equation 6 with $\varepsilon(r)$ from Figure 12a and $\sigma(r)$ from Equation 7. In calculating $\sigma(r)$, $\alpha = 1$ was selected as a worst case because (1) for $\alpha < 1$ the discrepancy between ideal and actual is smaller and (2) for $\alpha > 1$ (or $R/R_0^N \gtrsim 2$) the fuel tube is rejected despite the discrepancy.

With $\alpha = 1$ the maximum discrepancy between ideal and actual R/R_0^N is 1.5% for FWHM >0.3a. (High density areas smaller than this do not require density appraisal). Thus, the predicted collimator leakage effects are relatively small.

Measurements examined the denominator of Equation 6, as a function of collimator radius a, viz.

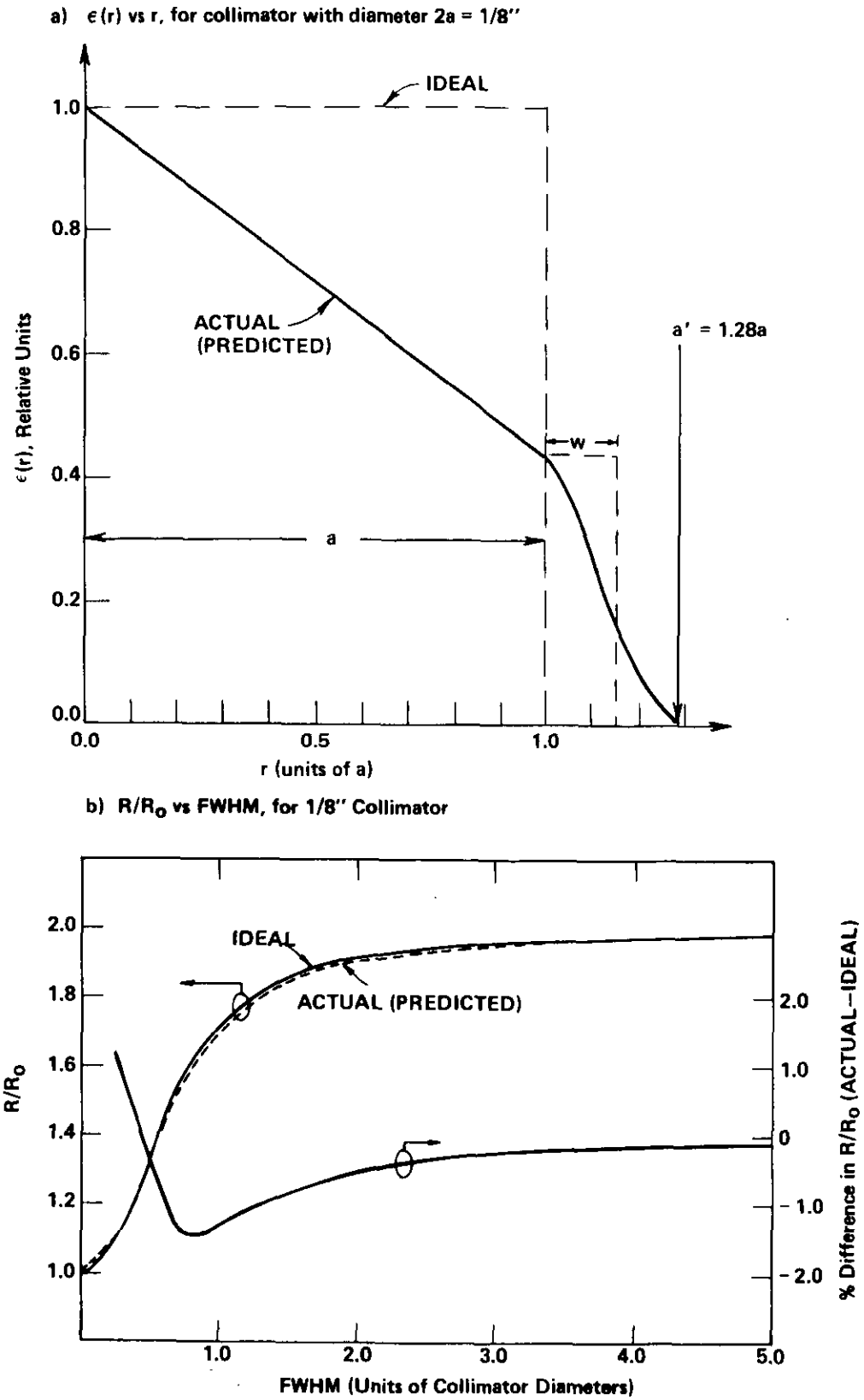

FIGURE 12. Calculation of R/R_0 for Collimator With Ideal $\epsilon(r)$ and Model-Predicted $\epsilon(r)$. Here $\sigma(r)$ is from Equation (7) with $\alpha = 1$.

$$R_0^N = \int_0^a \varepsilon(r)\ \sigma_0^N\ 2\pi r dr + \int_a^\infty \varepsilon(r)\ \sigma_0^N\ 2\pi r dr$$

$$= \sigma_0^N\ (\varepsilon_1\ \pi a^2 + \varepsilon_2\ 2\pi a w) \qquad (8)$$

where the first term represents detection within the collimator ($r<a$) and the second term represents leakage detection beyond the collimator ($r>a$) in an annulus of effective width w. ε_1 and ε_2, the effective detector efficiencies of the two regions, are treated as constants because they have only minor dependence on a for the range of collimator sizes examined. A plot for $R_0^N/\sigma_0^N\pi a^2$ vs 1/a tests Equation 8 in the form

$$R_0^N/\sigma_0^N\pi a^2 = \varepsilon_1 + 2\ \varepsilon_2 w\ (1/a) \qquad (8')$$

as shown in Figure 13. Here the normalized data yield an exceptionally good fit for Equation 8. The best least square fit yields $\varepsilon_1 = 0.624 \pm 0.055$ and $2\varepsilon_2 w = 0.0085 \pm 0.0047$ in. For comparison, the parameters $\varepsilon_1 = 0.627$ and $2\varepsilon_2 w = 0.0084$ in, were calculated from the integrals of Equation 8, using the model-predicted value of $\varepsilon(r)$. Actually, only the measured ratio of leakage to nonleakage, or $2\varepsilon_2 w/\varepsilon_1$ can be compared with calculation, because the data of Figure 12 are normalized to yield ε_1.

These experimental checks are consistent with the modeling used for $\varepsilon(r)$. Because the $\sigma(r)$ modeling spans an essentially complete range of cases (FWHM's), experimental checks on $\sigma(r)$ were deemed unnecessary. These aspects of $\varepsilon(r)$ and $\sigma(r)$ strongly argue that the good collimator performance predicted by the model calculation is actually obtained.

3.4 FGD Compared to FDA and Fluoroscope

Prior to developing the FGD, Pu density measurements were performed only with the FDA and the fluoroscope.[3] Both of these latter instruments utilize x-ray transmission measurements, as opposed to the plutonium gamma-ray measurements of the FGD. A comparison of density measurements for these instruments provides consistency appraisal for the FGD performance.

The FDA can examine densities for a minimum area of 1/4-inch x 1/4-inch. One tube examined had two large area hot spots that could be examined by both the FGD or the FDA. These measurements for the FGD with 1/4-inch diameter collimator and the FDA with 1/4-inch x 1/4-inch window are compared in Figure 14. In addition, two predictable measurements are compared as points as well:

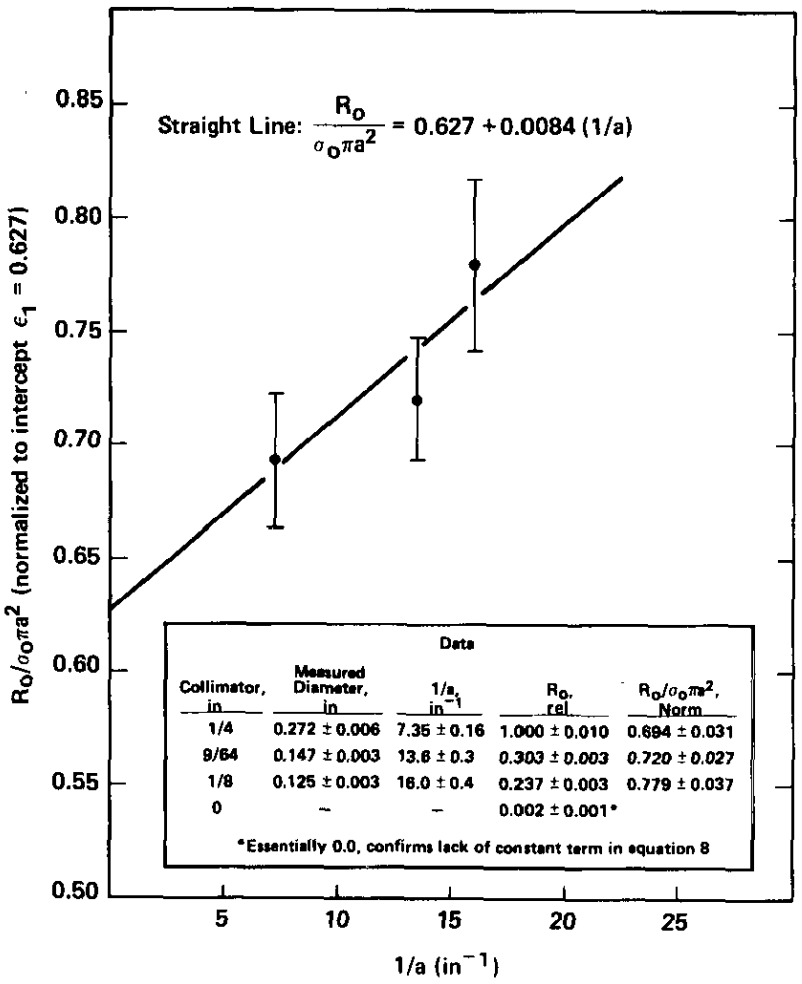

FIGURE 13. Measurements for Appraising Collimator Leakage

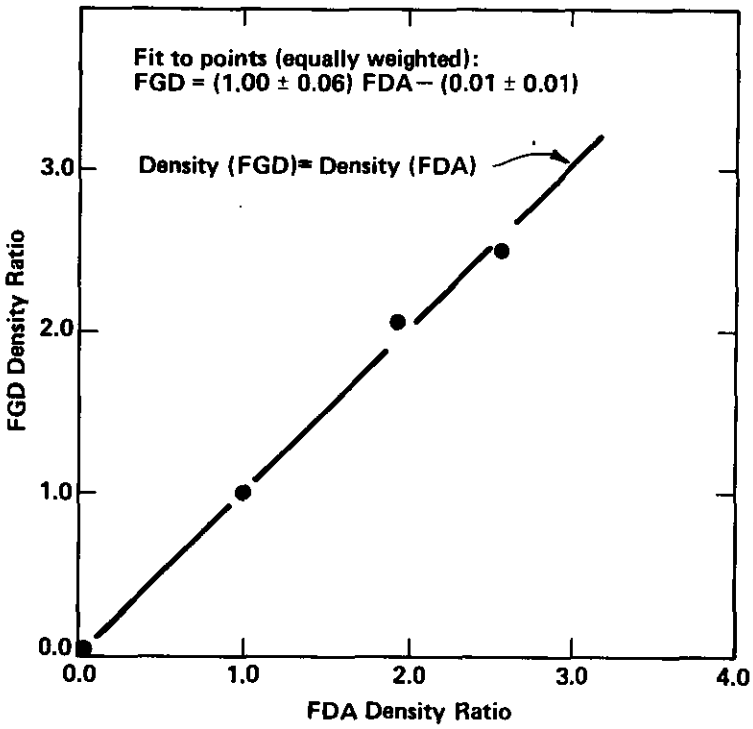

FIGURE 14. Comparison of FGD and FDA Measurements (with 1/4" Collimator)

(1) the density for a normal tube area (≡1 for FGD and FDA), and (2) the density for no PuO_2 (≡0 for FGD and FDA). These four points imply that FGD and FDA measurements for the larger areas agree quite well, as indicated in the figure. However, it is worth noting that FGD measurements with the 1/8-inch-diameter collimator generally yield higher densities than those obtained with the 1/4-inch-diameter collimator, as indicated in Figure 15. Thus, these smaller area FGD measurements resolve the peak PuO_2 densities better than the FDA and permit a more meaningful tube appraisal.

Measurements with the FGD (1/8-inch collimator) and fluoroscope are compared in Figure 16. The fluoroscope densities are determined somewhat subjectively, by visually comparing the spot "grayness" to the "grayness" of calibrated density gauges viewed with the fluoroscope. "Grayness" ranging from 1 (high density) to 4 (low density) is determined. The corresponding D values of the FGD display a definite correlation between fluoroscope and FGD measurements; however, the uncertainties associated with individual comparisons do not warrant direct calibration of the fluoroscope to FGD measurement.

The fluoroscope readings for high density areas near the center of the fuel tube (Figure 16a) correlate with larger FGD readings than the measured FGD readings for such areas near the end of the tube (Figure 16b). This results because the overall fuel density tapers off near the end of the tube and thus the fluoroscope density measured relative to this lower background density would be conservatively high. Both correlations show that the fluoroscope acceptance criterion (fluoroscope densitites must be >3) are conservative since the corresponding FGD values of D are relatively small (<1.4) compared to acceptance criteria discussed in Section 4.1 below.

4.0 APPLICATIONS

4.1 Appraisal of Hot Spots

Tubes with high fuel density areas can experience clad corrosion and/or localized melting at hot spots, when irradiated in a Reactor. An x-radiograph of a typical hot spot is shown in Figure 17. A number of SRP-produced fuel tubes were determined recently to have high density PuO_2 areas, per measurements with the FDA and fluoroscope. The FGD examined these areas in closer detail, so that the maximum densities of these areas could be identified using the resolution of the 1/8-inch diameter collimator. These maximum density measurements were then compared with calculated acceptance limits, to establish the tube quality.[4] Tube quality classes of A, B, and C were assigned for acceptable tubes on a best, average, and worst basis. Unacceptable tubes were class F. This quality

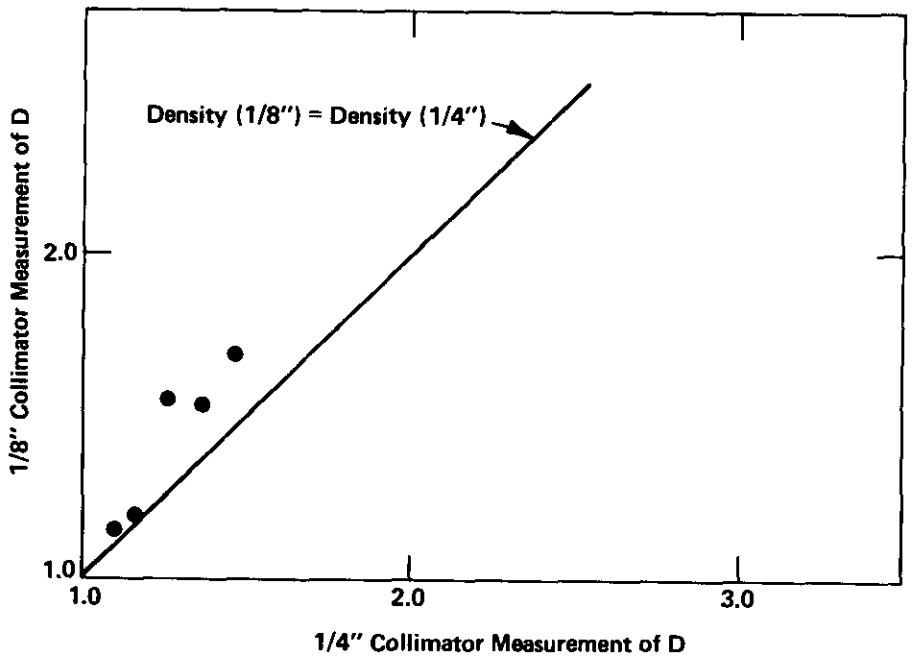

FIGURE 15. Comparison of FGD Densities Measured with 1/8" and 1/4" Collimator

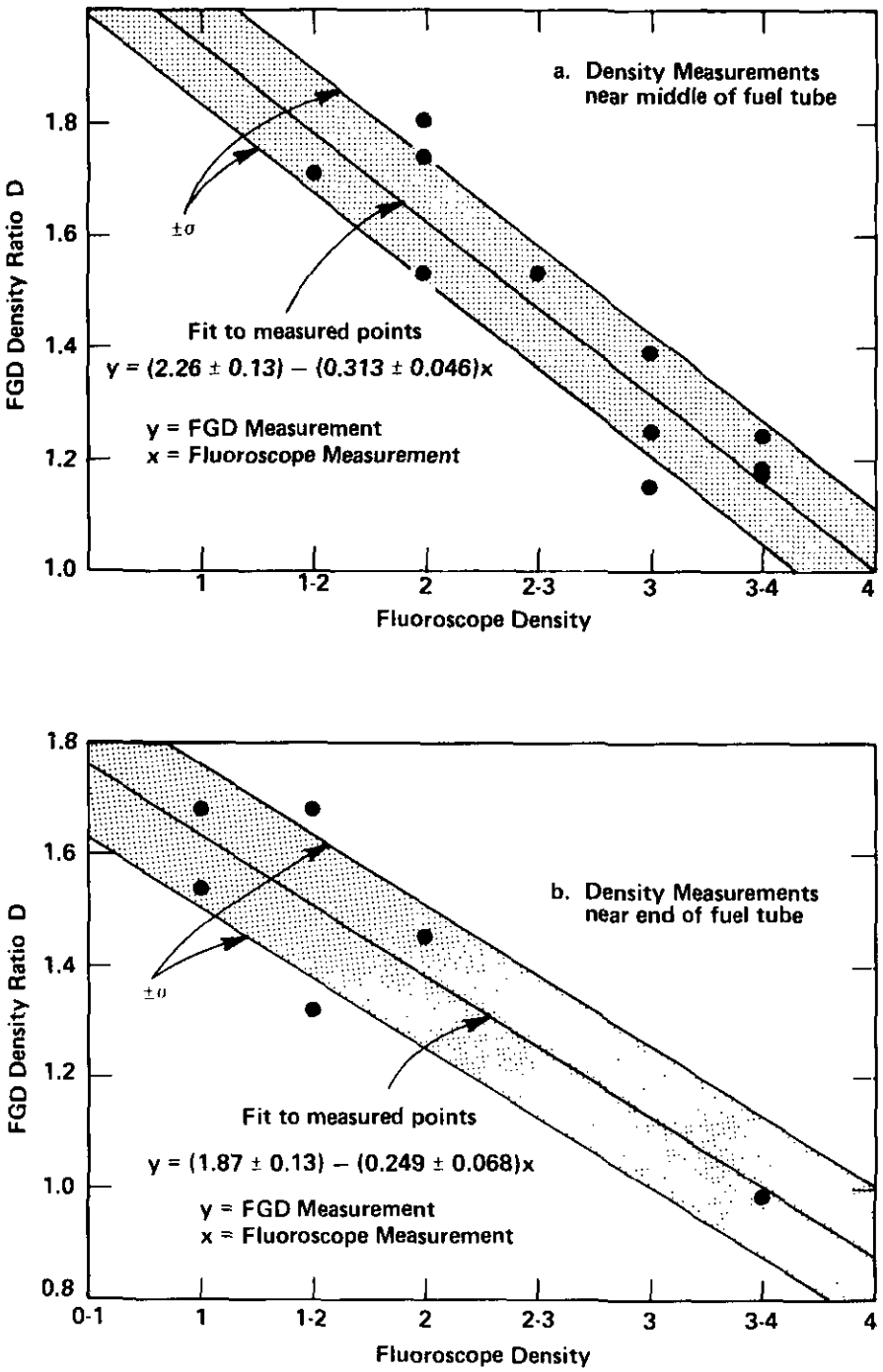

FIGURE 16. FGD vs. Fluoroscope Performance (1/8" Collimator)

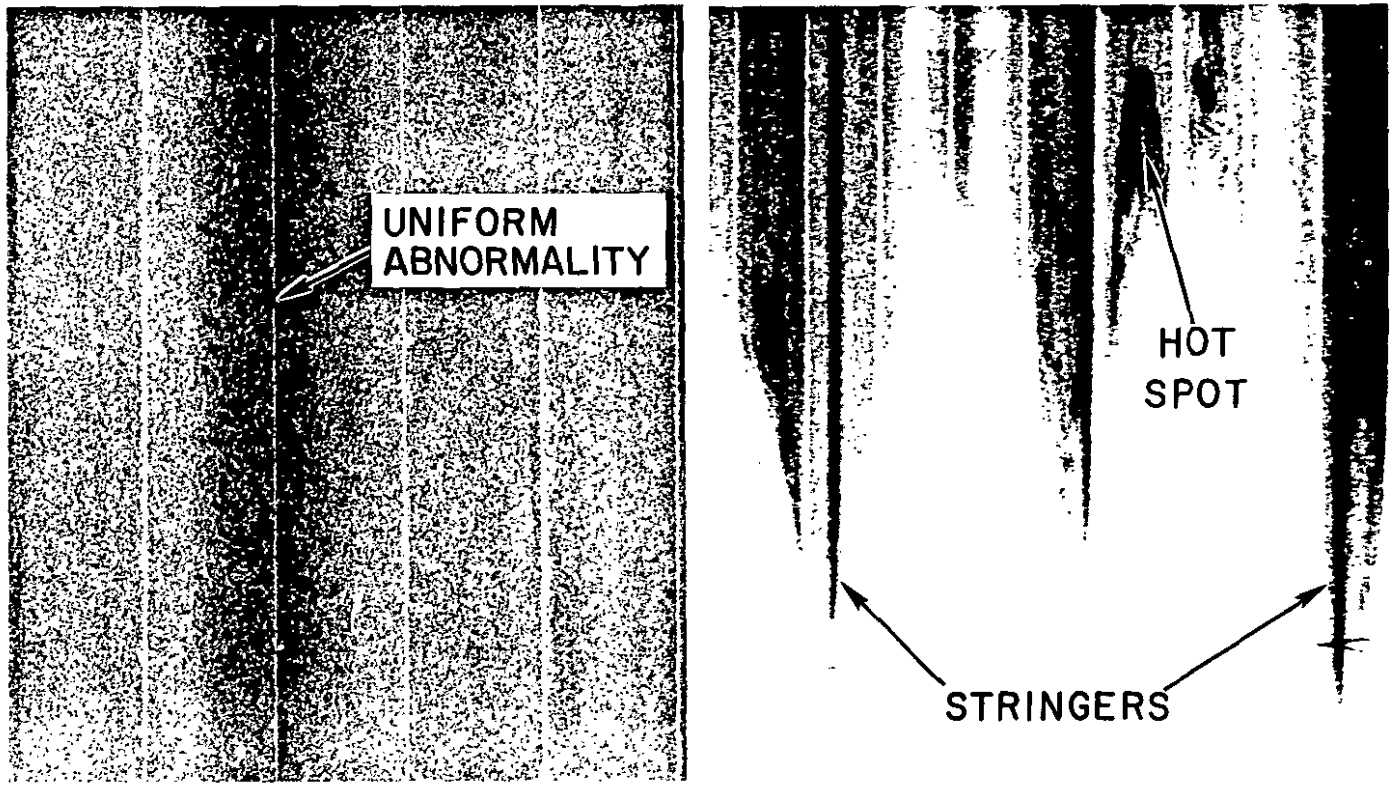

FIGURE 17. Radiographs of Various Regions of Fuel. These Radiographs Were Exposed in Contact With the Inside of the Tube, so that the Tube Appears "Unwrapped" about its Circumference

classification determines where the tubes can be safely placed in the reactor, relative to neutron irradiation levels. For example, a class C tube must be located near the edge of the reactor, where the neutron flux is relatively low.

Figure 18 summarizes the results of the 19 tubes appraised for hot spots in this study. The FGD measurements indicated that 14 of these tubes were acceptable. To be conservative relative to the quality-acceptance limits, the FGD values of $D_{max} = D + \Delta D$ were used in these appraisals. These FGD results, along with other tube tests, were used in selecting the fuel to be loaded in the reactor.

4.2 Analyses of High Content Over Large Area

An unusually large area of abnormally high but essentially uniform PuO_2 density was indicated in an x-radiograph of one outer tube, as shown in Figure 17. It was important to analyze this feature so that the cause of this deviation could be identified and prevented in the tube manufacturing process. Such a high density region could be caused by (1) cladding thinning, which is accompanied by a larger PuO_2-Al fuel thickness, (2) incomplete homogenization of PuO_2 and Al, yielding PuO_2-Al that is abnormally high in PuO_2, or (3) some combination of these two possibilities. Thus, a complete appraisal required measurements with FGD and the cladding thickness monitor.[18]

The following analysis of the measurements indicates that cladding thinning alone accounts for the large area high density region. For this region, outer clad thickness $T_c = 0.0095 \pm 0.0015$ inch and inner clad thickness $T_c' = 0.0277 \pm 0.0015$ inch were measured with the cladding thickness monitor. From Table I, the total thickness of an outer tube is $t_c + t_0 + t_c' = 0.133$ inch; thus, the thickness of the examined PuO_2-Al region is $T_0 = 0.133 - T_c - T_c' = 0.0958 \pm 0.021$ inch. The gamma count rate from this uniform PuO_2 region is, from Equation 1

$$R_0(T_0) = e^{-\mu_a T_c} \int_0^{T_0} \epsilon A_c e^{-U_0 X} P_0 dX$$

where:

U_0 = value of μ_0 for region T_0

P_0 = value of ρ_0 for region T_0

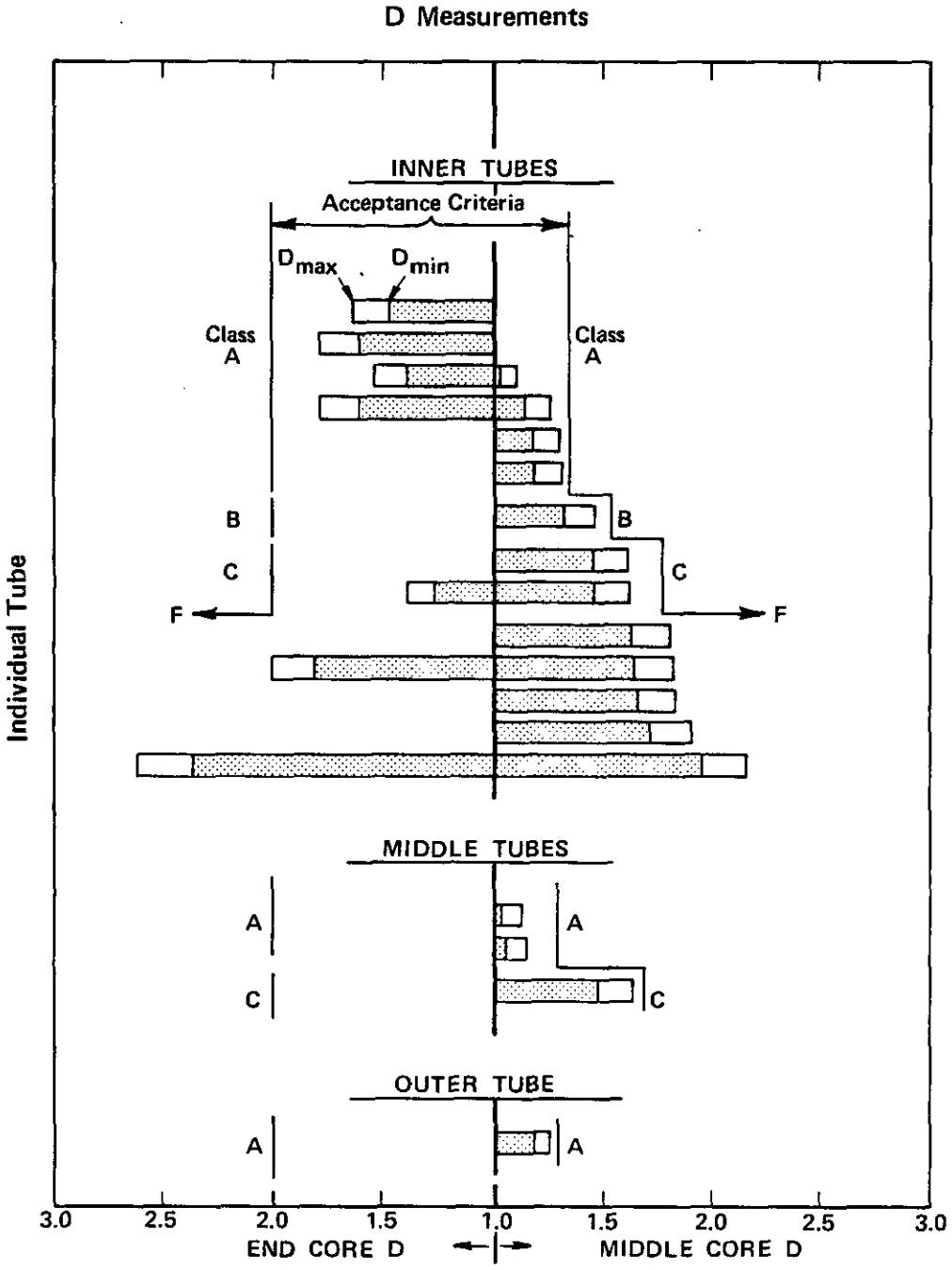

FIGURE 18. Results of "Hot Spot" Measurement, as Classified by Tube Quality Class. Only the Highest Density "Hot Spots" are Shown for a given tube and core region

The ratio $R_0(T_0)/R_0(t_0)$ was calculated in terms of P_0/ρ_0^N and then set equal to the $R_0(T_0)/R_0^N(t_0) = 1.320 \pm 0.017$ measured with the FGD. This yielded $P_0/\rho_0^N = 1.023 \pm 0.025$, where the error includes the uncertainty in T_0. Thus, the PuO_2 densities of the normal and tested regions agree well, and the difference in count rates $R_0(T_0)$ and $R_0^N(t_0)$ is solely due to cladding thickness effects.

4.3 Study of Fuel Distributions Near Tube End

Abnormalities in PuO_2 density and cladding thickness are most frequent near the tube end region containing the end core and stringers. As shown in Figure 19, the end core is the core boundary region at the finally extruded end of the tube. A stringer is composed of fuel that appears to "back-extrude" out of the core. When cladding thinning exists in these regions, the tube may still be acceptable if the PuO_2 density is sufficiently low. Thus, a study of PuO_2 density distributions within these regions serves to indicate whether the frequency of unacceptable thin clad tubes warrants any changes in the manufacturing process.

FGD measurements for randomly selected end core areas and stringers are summarized in Figures 20 and 21. These measurements indicated that PuO_2 densities within the end core are essentially uniformly distributed between $D_0 = 0.0$ and 1.0; however, although not observed in these measurements, an occasional hot spot still could lie well above this range. All measurements of stringers yielded $D_0 < 0.5$. Because these results indicate that D is appreciably less than 1.0 for most cases, the necessity for rejecting tubes with cladding thinning in the end core and stringer regions is not expected to be frequent. However, appraisal of individual cases should be made to establish acceptability.

5.0 CONCLUSIONS

5.1 General

The FGD reliably measures PuO_2 densities within 1/8-inch-diameter areas of SRP fuel tubes, by monitoring the 208 keV gamma from the ^{241}Pu decay chain. The same instrument and technique should be applicable in measuring U-densities of similar tubular fuel. Here the 186 keV gamma from ^{235}U can be monitored.[1,2,9]

5.2 Possible Improvements

The current FGD is strictly a prototype, and a number of improvements are possible. Among these are computerized peak

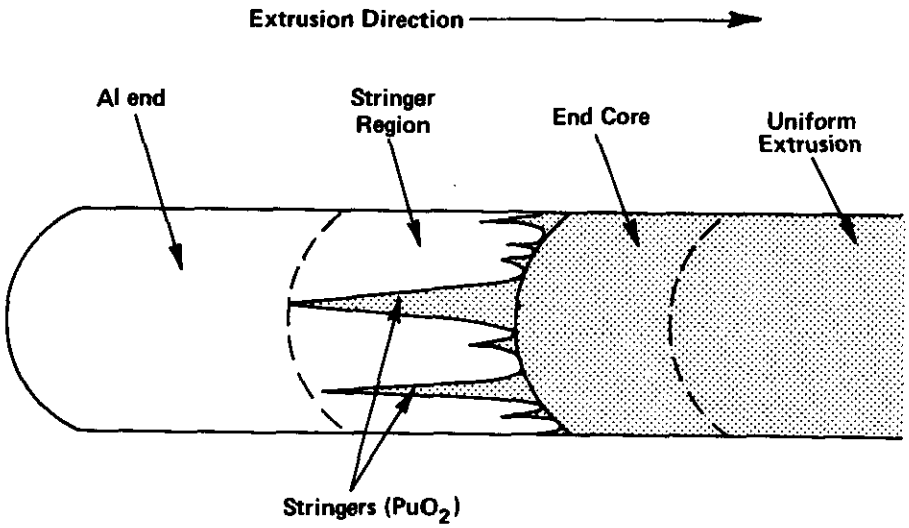

FIGURE 19. Regions Near End of Fuel Tube

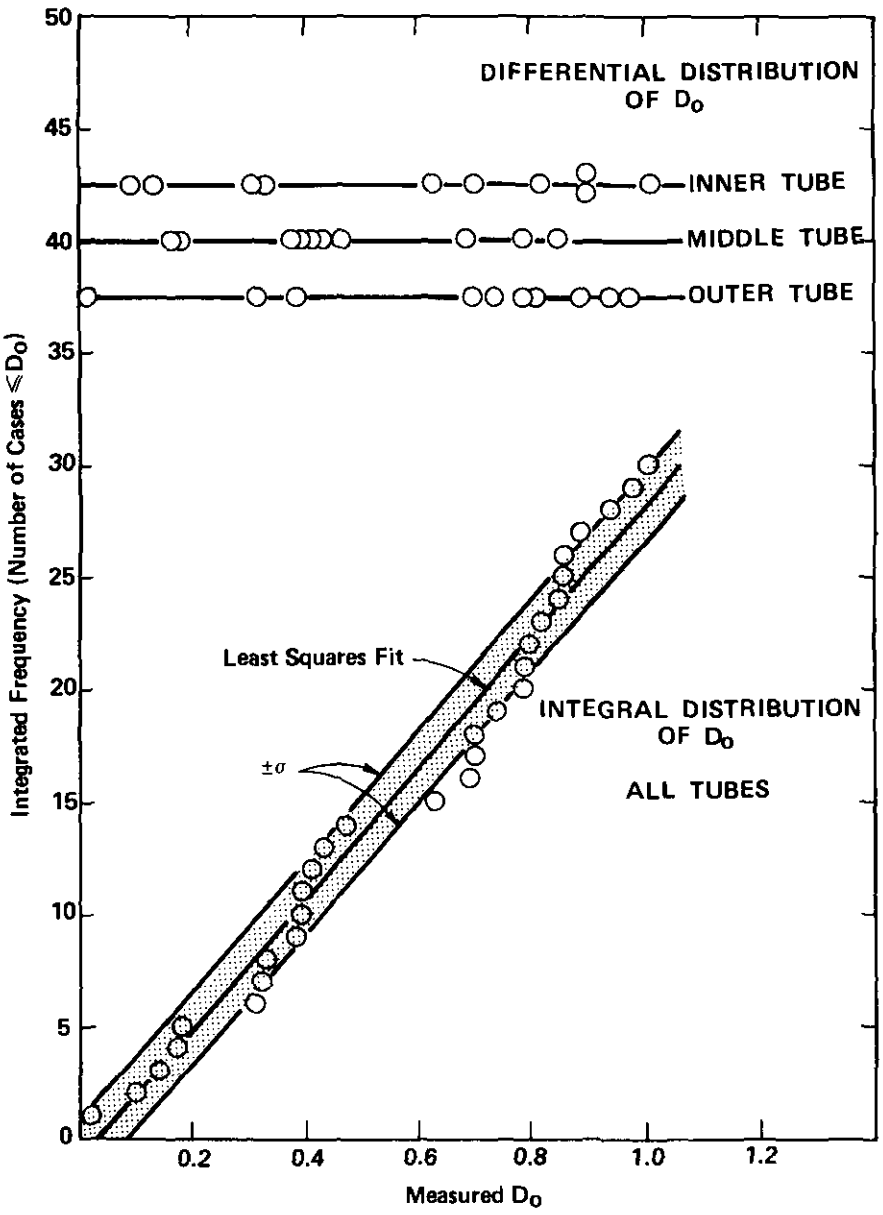

FIGURE 20. D_0-Measurements for End Cores of Tubes. The Linear Character of the Integrated Frequency of D_0 Indicates that D_0 is Essentially Uniformly Distributed Between 0.0 and 1.0

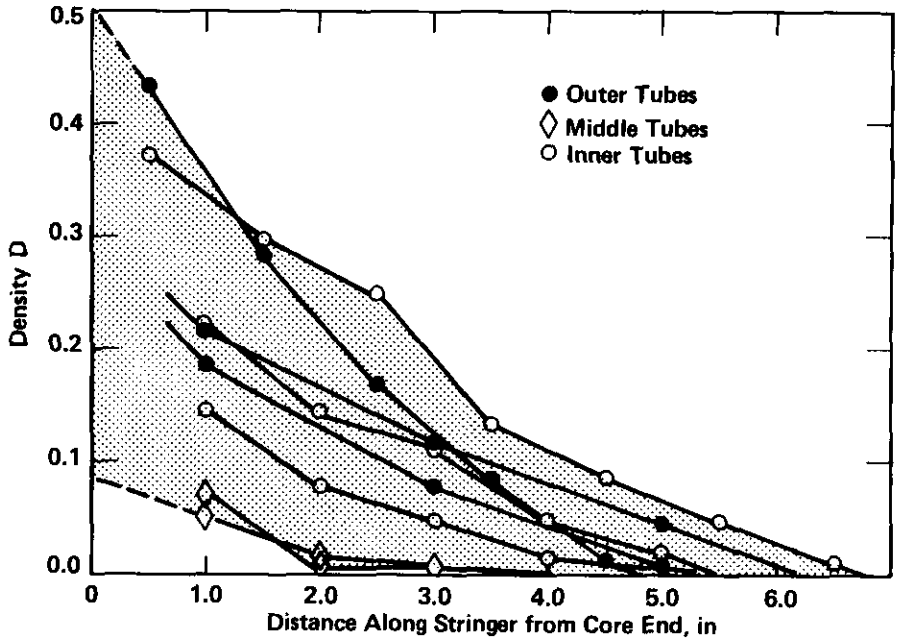

FIGURE 21. D_0-Measurements for Stringers

analysis for D, automated density mapping, and reduction of the $\pm\Delta D$ uncertainty. Obvious solutions exist for all but the last item.

The $\pm\Delta D$ uncertainty may be reduced by measuring R/R_0^N for more than one gamma ray in the spectrum.[19] For example, R/R_0^N can be measured for the 208.0 keV gamma ray of the $^{241}Pu \rightarrow {}^{237}U$ decay mode and the 59.5 keV gamma from the $^{241}Pu \rightarrow {}^{241}Am$ decay mode.[1-2] Both of these gammas will experience minimum and maximum attenuations for the same extremes of source geometry, given in Figure 5. In Figure 22, R/R_0^N (208.0 keV) vs R/R_0^N (59.5 keV) for these extremes are plotted parametrically against D_{min} and D_{max}, using Equation (4a) and (4b). A measured R/R_0^N (208.0 keV) and R/R_0^N (59.5 keV) define a point lying between the two extreme curves and along some characteristic $D = D_{max} = D_{min}$, which defines the density ratio. This measurement of D is clearly more precise than the $D \pm \Delta D$ defined between the curves by only a R/R_0^N (208.0 keV) measurement. In essence, the two R/R_0^N values yield information on the density ratio and the PuO_2 positional distribution in the high density spot. Such a technique would be useful for fuel tubes with greater self absorption.

For the application of the present work, R/R_0^N (208.0 keV) measurements alone were adequate; however, some data concerning the feasibility of the two-gamma-monitoring were obtained. Density mappings included count rates for windows about both 59.5 keV and 208.0 keVpeaks, as discussed in Figure 10. These count rates should be corrected for background within the window for proper D analysis with Figure 22. Nevertheless, these results yield approximate values of R/R_0^N(59.5 keV) and R/R_0^N (208.0 keV) that are consistent with the attenuation effects predicted in Figure 22. These measurements and Figure 22 also show that for single-gamma-monitoring, the 208.0 keV gamma is superior to the 59.5 keV gamma, as the $\pm\Delta D$ is much smaller for the 208.0 keV case.

5.3 Applicability

The FGD technique was developed to appraise fuel densities of tubular fuel. For hot spot analyses, the fuel annulus of the tube must be thin enough to permit minor γ-shielding corrections. This study yielded D values limited to 3 to 5% uncertainty due to γ-shielding, which corresponds to low (~0.05) volume fraction PuO_2 within thin (~0.1 inch) fuel annuli. Thus, the method may not be applicable to hot spot examination for fuel in pellet form, as such fuel typically will have much larger γ-shielding effects. For cases not involving hot spots, where fuel geometry and uniformity are known, the method is not limited by γ-shielding uncertainties.

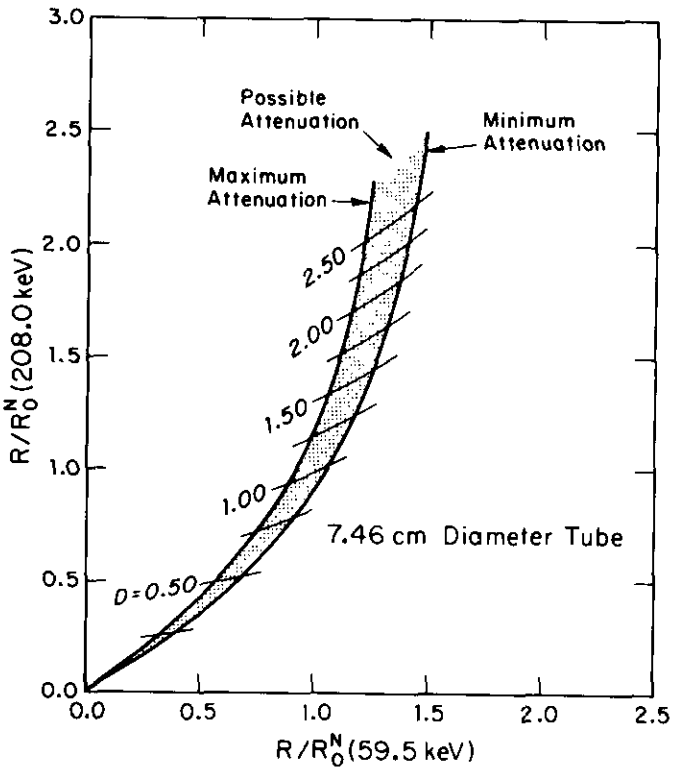

FIGURE 22. Use of 208.0 keV and 59.5 keV Gamma for Precise D Measurement. (Plot applies for Middle Tube for a Given Tube and Core Region.)

6.0 ACKNOWLEDGMENTS

The author wishes to thank R. L. Frontroth and D. R. Johnson for acquainting him with the need for developing an instrument such as the FGD. Useful discussions and suggestions were rendered by them and H. B. Peacock, N. P. Baumann, K. J. Hofstetter, and P. H. Stevens. Experimental and equipment assistance from M. Hendrix, J. D. Stewart, and R. S. Sullivan is also gratefully acknowledged.

7.0 REFERENCES

1. R. Gunnink, J. E. Evans, and A. L. Prindle. A Re-Evaluation of the Gamma-Ray Energies and Absolute Branching Intensities of ^{237}U, $^{238,239,240}Pu$ and ^{241}Am. USERDA Report UCRL-52139 Lawrence Livermore National Laboratory, Livermore, CA (1976).

2. Table of Isotopes. 7th Edition, C. M. Lederer and V. S. Shirley, eds., John Wiley & Sons, Inc. (1978).

3. M. W. Tarpley. Semi-Automatic Fluoroscope. Report DPSPU-76-30-14, E. I. du Pont de Nemours & Co., Savannah River Plant, Aiken, SC (1976).

4. D. R. Muhlbaier, Savannah River Laboratory, personal communication.

5. R. Sher and S. Untermeyer, II. The Detection of Fissionable Materials by Nondestructive Means. p. 119. The American Nuclear Society, LaGrange Park, IL (1980).

6. W. D. Ruhter and D. C. Camp. Nondestructive Assay of Mixed Uranium - Plutonium Oxides by Gamma-Ray Spectrometry. USDOE Report UCRL-52625, Lawrence Livermore National Laboratory, Livermore, CA (January 1979).

7. R. Gunnink. Gamma Spectrometric Methods for Measuring Plutonium. USDOE Report UCRL-80464, Lawrence Livermore National Laboratory, Livermore, CA (February 16, 1978).

8. Determination of Uranium and Plutonium in Nuclear Fuels. Herbert Sorantin, ed., pp. 27-39, Verlag Chemie, New York (1975).

9. W. A. Higinbotham. Passive Gamma-Ray Scanning of Plutonium Recycle Fuel Rods. USAEC Report BNL-50351, Brookhaven National Laboratory, Long Island, New York, (June 1972).

10. R. Gunnink and J. F. Tinney. "Analysis of Fuel Rods by Gamma-Ray Spectrometry." Symposium on Analytical Methods in Nuclear Fuel Cycle, IAEA, Vienna, 1972. USAEC Report UCRL-51086, Lawrence Livermore National Laboratory, Livermore, CA, p. 373 (August 1971).

11. R. W. Brandenburg, N. S. Beyer, and R. B. Perry. "Nondestructive Assay of Plutonium Reactor Fuel by Gamma Ray Measurements Using On-Line Computer Control." Materials Evaluation 28, 77 (1970).

12. G. R. Keepin, et al. "Application Areas and Results of Non-Destructive Assay Measurements." Proc. IAEA Symposium on Progress in Safeguards Techniques, II, Vienna, 79 (1970).

13. J. Gerard and L. Van Hove. "Determination of the Uranium Content of Aluminum Alloys." Symposium on Non-Destructive Testing in Nuclear Technology, Bucharest, 1965. IAEA Proceedings Series, Vol. I, p. 35 (1965).

14. W. C. Francis, et al. "The Role of Non-Destructive Testing in Test-Reactor Operation at the National Reactor Testing Station." Symposium on Non-Destructive Testing in Nuclear Technology, Bucharest, 1965. IAEA Proceedings Series, Vol. II, p. 331 (1965).

15. P. Libotte, H. Inniger, and J. M. LeBlanc. "Non-Destructive Testing of Plutonium-Enriched Fuel Rods." Symposium on Non-Destructive Testing in Nuclear Technology, Bucharest, 1965. IAEA Proceedings Series, Vol. I, p. 101 (1965).

16. Plutonium Handbook. O. J. Wich, ed., p. 763, Gordon & Breach, Science Publishers, Inc., New York (1967).

17. J. H. Hubbel. Photon Cross Section Attenuation Coefficients from 10 keV to 1 GeV. National Bureau of Standards Report NSRDS-NBS-29 (1969).

18. R. V. Slates and W. E. Stewart. Measurement of Reactor Tube Cladding Thickness by X-Ray Fluorescence Spectrometry. USDOE Report DP-1465, E. I. du Pont de Nemours & Co., Savannah River Laboratory, Aiken, SC (January 1978).

19. J. L. Parker and T. D. Reilly. "Bulk Sample Self-Attenuation Correction by Transmission Measurement." Proc. ERDA X- and Gamma-Ray Symposium, Ann Arbor, MI, May 19-21, 1976. CONF 760539 (1976).